EPJ Web of Conferences **29**, 00031 (2012)
DOI: 10.1051/epjconf/20122900031

Crystal structure, NMR study, dc-conductivity and dielectric relaxation studies of a new compound $[C_2H_{10}N_2]Cd(SCN)_2Cl_2$

K. Saidi [a,1], S. Kamoun [a], H. F. Ayedi [a] and M. Gargouri [b]

[1] Laboratoire de Génie des Matériaux et Environnement, ENIS, 1173, Université de Sfax, Tunisia
[2] Laboratoire de l'état solide, Faculté des sciences de Sfax, B.P.1171, 3000 Sfax, Tunisia

Abstract. The crystal structure, the solid NMR spectroscopy and the complex impedance study have been carried out on $[C_2H_{10}N_2]CdCl_2(SCN)_2$. Characterization by single crystal X-ray crystallography shows that the cadmium atoms have à 2N2S2Cl hexa-coordination sphere, exhibiting pseudo-octahedral geometry. The cadmium atoms are bridged by two thiocyanate ions generating 1-D polymeric-chains. These chains are themselves interconnected by means of N-H…Cl(NCS) hydrogen bonds originating from the organic cation $[(NH_3)_2(CH_2)_2]^{2+}$. ^{111}Cd isotropic chemical shifts span a range of 268ppm. The cadmium atom exhibits multiplets that result from ^{111}Cd-^{14}N spin-spin coupling. Examination of ^{111}Cd and ^{13}C MAS line shapes shows direct measurement of the indirect spin-spin coupling constant $^2J(^{111}Cd,^{14}N)$ = 105Hz and the dipolar coupling constant of 1381Hz . Impedance spectroscopy measurements of $[C_2H_{10}N_2]CdCl_2(SCN)_2$ have been studied from 209Hz to 5 MHz over the temperature range 300-370 K. The Cole-Cole (Z'' versus Z') plots are fitted to two equivalent circuits models. The formalism of complex permittivity and impedance were employed to analyze the experimental data. The dc conductivity follows the Arrhenius relation with an activation energy E_a = 0.54 (3) eV.

1 Introduction

Organometallic complexes based on cadmium-thiocyanates have attracted a great research attention because they exhibit excellent physical properties such as nonlinear optical (NLO) behavior. These materials coupling the ambidentate nature and bridging capacity of thiocyanates with the thermal stability, structural diversity and simplicity in processing of organic molecules can enlarge their field of applications [1]. Thiocyanate and isothiocyanate anions can coordinate through either the nitrogen or the sulfur atom or both to the metal center. Cd(II) has the particularity to exhibit both (S and N) bonding modes to $(SCN)^-$ ligands tending to form a 6- coordinated octahedral complexes.

In this paper we report the synthesis, the crystal structure, the heteronuclear ^{111}Cd, ^{13}C CP/MAS NMR spectroscopy and impedance spectroscopy of a novel 1-D coordination array $[C_2H_{10}N_2]CdCl_2(SCN)_2$. The impedance spectroscopic measurements were performed in a wide temperature range from 300 to 370 K. the electrical relaxation analysis was performed using the

[1] e-mail : khaoulaslaheddine@yahoo.fr

conductivity $\sigma^*(\omega)= \sigma'(\omega)+ i\sigma''(\omega)$ and dielectric $\varepsilon^*(\omega)= \varepsilon'(\omega)+ i\,\varepsilon''(\omega)$ formalism. The temperature and frequency dependence of the dielectric properties of the compound is reported.

2 Experimental

Crystals of ethylenediammonium bis chloro diisothiocyanato cadmium (II) were prepared by dissolving in aqueous medium a stoichiometric mixture of Cd $(SCN)_2$ and ethylenediammonium dichloride according to the following chemical reaction.

$$C_2H_{10}N_2Cl_2 + Cd(SCN)_2 \rightarrow [C_2H_{10}N_2]CdCl_2(SCN)_2 \quad (1)$$

The experimental conditions used for the single crystal data collection are reported in Table1. All calculations were performed using SHELXL-97 [2] computer programs included in the WINGX software package [3]. The structural figures were carried on with Mercury 2.3 supplied by crystal impact [4]. The atomic scattering factors were taken from the International Tables for X-ray Crystallography [5]. The structure was solved by the heavy–atom method. The position of nitrogen, sulfur and chlorine atoms were deduced from their three-dimensional Patterson maps using the SHELXS-97 program, while the remaining other atoms were located by means of successively Fourier maps. Full matrix refinement with anisotropic thermal parameters for all non-hydrogen atoms and isotropic thermal parameters for H atoms converged to a final R value of 0.0249.

^{13}C and ^{111}Cd solid-state NMR spectra were recorded on a BRUKER 300MHz (7.1T) spectrometer using cross polarization (CP) and magic- angle spinning(MAS) with 63.633 MHz Larmor frequency for ^{111}Cd and 75.467 MHz for ^{13}C. Impedance spectroscopy measurements have been carried out from 209Hz to 5MHz over the temperature range 300-370K using a TEGAM 3550 ALF automatic bridge monitored by a micro-computer. Crystallographic data for the structure reported in the paper (excluding structure factors) have been deposited with the Cambridge Crystallographic Data Centre, CCDC, no 818072 in the European Physical Journal.

3 Results and discussion

3.1 Structure description

Figure1 shows the ORTEP drawing of the molecular structure of $[C_2H_{10}N_2]CdCl_2(SCN)_2$ with the atom numbering scheme, while Figure2 and Figure3 shows the 1D network character of the complex. Selected bond distances and bond angles are listed in table2. The structure consists of doubly SCN-bridged 1-dimensional chains along the crystallographic (100) direction (Figure2). Each cadmium atom is pseudo-octahedrally coordinated by two trans-coordinated chloride anions, two trans-arranged sulfur atoms and two trans-arranged nitrogen atoms from the bridging thiocyanate groups. The double bridging action of SCN^- gives rise to eight-membered $Cd_2(SCN)_2$ rings in the chair conformation because of the almost linear SCN group (S-C-N = 179.0(3)). The centeroid of the rings is a center of inversion. These chains build up the 1D chain through their corner-sharing action at two cadmium atoms. Weak intrachain N-H…NCS and N-H…Cl hydrogen bonds are

formed from each ethylenediammonium groups to the nitrogen and chlorine donor atoms of the $[CdCl_2(SCN)_2]_n^{2-}$ anionic chains.

Table 1. Crystal data and structure refinement for $[C_2H_{10}N_2]$ Cd Cl_2 $(SCN)_2$

Empirical formula	$[C_2H_{10}N_2]$ Cd Cl_2 $(SCN)_2$
Colour, Shape	Colorless, cubic shape
Formula weight	361.58
Temperature (K)	298 (2)
Crystal system	Monoclinic
Space group	P2/c
a (Å)	7.2745(10)
b (Å)	7.4183(10)
c (Å)	10.9116 (20)
β (°)	98.268(10)
No. of reflections collected	2358
No. of independent reflections	1248
Goodness-of fit on f^2	1.117
R indices [I>2σ (I)]: R (%); WR_2 (%)	0.0249 ; 0.0312

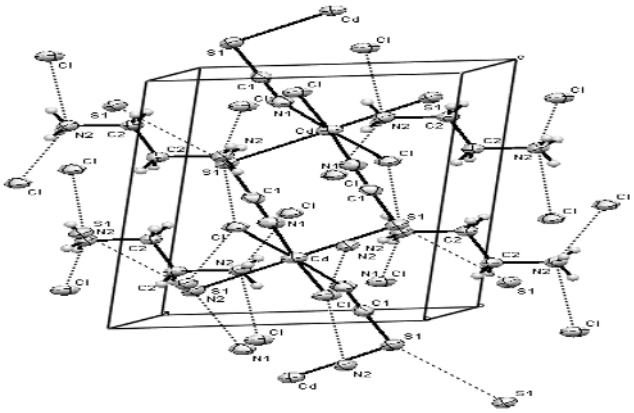

Fig.1. ORTEP stereoscopic projection of the crystal packing.

Table 2. Principal intermolecular distances (Å) and bond angles (°)

Atome	**Distances**	**Atome**	**Angles**
Cd – S(1) :	2.7689(4)	N (1) – Cd – S(1) :	89.75(0)
Cd – $S(1)^{(j)}$:	2.7689(4)	Cl – Cd – S(1) :	93.13(0)
Cd – Cl :	2.5653(3)	$Cl^{(j)}$ – Cd – S(1) :	89.08(3)
Cd – $Cl^{(j)}$:	2.5653(3)	$S(1)^{(j)}$ – Cd – S(1):	176.87(4)
Cd – N(1):	2.3710(3)	$Cl^{(j)}$ – Cd – N(1):	92.00(9)
Cd – $N(1)^{(j)}$:	2.3710(3)	$S(1)^{(j)}$ – Cd– N(1):	87.96(6)
N (1)–C(1):	1.1647(35)	$N(1)^{(j)}$ – Cd –N(1):	85.68(13)
N (2)–C(2):	1,157(7)	$Cl^{(j)}$– Cd – Cl:	90.46(4)
S (1)–$C(1)^{(i)}$:	1.6533(3)	$S(1)^{(j)}$ – Cd – Cl:	89.08(3)
S $(1)^{(i)}$ –C(1) :	1.6533(3)	$N(1)^{(j)}$ –Cd –S(1):	87.96(6)
$N(1)^{(j)}$ –Cd –C $l^{(j)}$:	176.24 (7)	N $(1)^{(j)}$ – Cd – C l:	92.00(7)
$N(1)^{(j)}$–Cd – $S(1)^{(j)}$:	89.75(6)	$S(1)^{(j)}$ – Cd – C $l^{(j)}$:	93.13 (3)
C(1)-S(1) $^{(j)}$ –N(1):	179.0(3)		

Symmetry Codes: (i) x, - y-1, z+1/2 ; (j) –x+1, y, -z+1/2

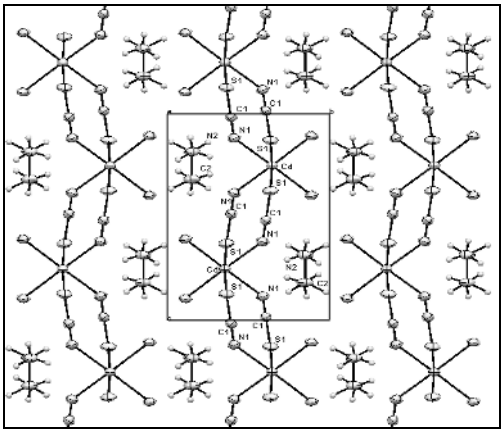

Fig.2. Projection along the a-axis of $C_2H_{10}N_2\ CdCl_2\ (SCN)_2$

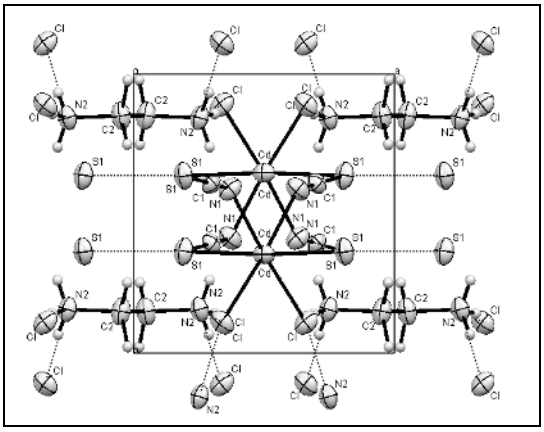

Fig.3. Projection along the c-axis of $C_2H_{10}N_2\ CdCl_2\ (SCN)_2$.

3.2 NMR Spectroscopy

The isotropic band of ^{111}Cd and ^{13}C, CP-MAS-NMR spectrum of the title compound rotating at magic angle with frequency 8000Hz are given in Figure 4 and Figure 5.

The ^{111}Cd CP/MAS NMR spectrum consists of five peaks of relative intensities 1:2:3:2:1 that indicate a coupling of ^{111}Cd with two ^{14}N nuclei [6]. The best agreement between the experimental and the calculated spectrum was achieved by introducing two equivalent ^{14}N nuclei with the same values of J=105Hz and d= -3. This is consistent with the structure determination by X-ray crystallography which indicates that the cadmium is surrounded octahedrally by two equivalent nitrogen, two sulfur atoms, and two chlorine atoms.

The ^{13}C CP/MAS NMR spectrum of $[C_2H_{10}N_2]CdCl_2(SCN)_2$ shows the existence of two signals, with the values of the isotropic chemical shifts 44.89 ppm and 129.16 ppm. These signals correspond respectively to the carbon atoms of the ethylenediammonium cation and the thiocyanate anion.

According to the literature on the solid state, the coupling between ^{13}C and ^{14}N is essentially due to the quadrupole interaction on the ^{14}N nucleus, and it appears as an asymmetric doublet (with intensity2:1) [7].

The splitting between the peaks due to the ^{14}N m=0 and m= ±1 spin states correspond to -3d, where d is the residual dipolar coupling [8] given by:

$$d = -\frac{3\chi^D}{20Z}(3\cos^2\beta^D - 1 + \eta\sin^2\beta^D\cos 2\alpha^D) \qquad (2)$$

with the quadrupolar coupling constant, $\chi = e^2Qq_{zz}/h$, the asymmetry parameter of the EFG tensor, $\eta=(q_{xx}-q_{yy})/q_{zz}$, and the Larmor frequency, $Z= \gamma_S B_0/2\pi$, of the spin-S nucleus. The dipolar coupling constant D is given by:

$$D = \left(\frac{\mu_0}{4\pi}\right)\frac{\gamma_I\gamma_S}{r_{IS}^3}\left(\frac{h}{2\pi}\right) \qquad (3)$$

and the azimuthal and polar angles, α^D and β^D define the orientation of the dipolar vector, r_{IS} with respect to the principal axis system of the EFG tensor.

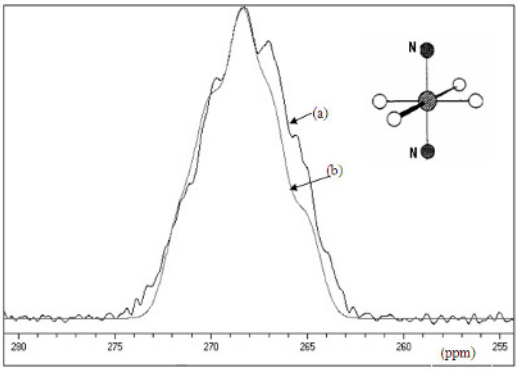

Fig.4. Isotropic region of the ^{111}Cd MAS NMR spectrum of $C_2H_{10}N_2$ $Cd(SCN)_2(Cl)_2$ having spin-spin coupling of ^{111}Cd to two ^{14}N nuclei: (a) experimental spectrum; (b): calculated spectrum.

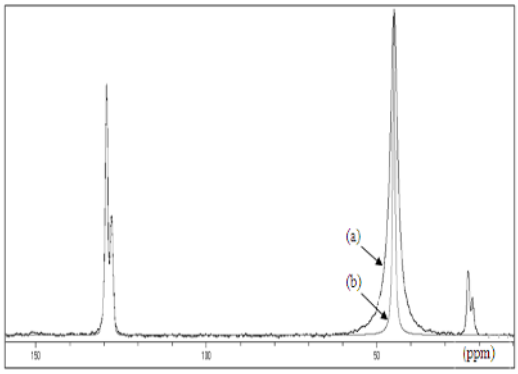

Fig.5. ^{13}C CP/MAS spectrum of $C_2H_{10}N_2$ $Cd(SCN)_2(Cl)_2$ having direct dipolar coupling to ^{14}N nuclei: (a) experimental spectrum; (b): calculated spectrum.

In our case, a splitting of 104Hz is observed, which corresponds to a value of d = -34.6Hz. These values are in agreement with those reported by Klauss Eichele et al. and Olivieri et al [8].

The spectrum was simulated using the ^{14}N, ^{13}C dipolar coupling constant for one site, D=1381Hz which correspond to r_{CN}= 1.165(4)Å and varying the quadrupole coupling constant χ (see figure 5).

3.3 Impedance analysis and equivalent circuit

Figure 6 shows typical complex impedance for $[C_2H_{10}N_2]CdCl_2(SCN)_2$ at some selected temperatures. In all the cases the experimental complex impedance plots a depressed semicircle was observed. Above 330K the depressed semicircles are accompanied by a straight line on the low frequency side, suggesting electrolyte-electrode polarization at the blocking electrode [9]. Such depression of the semicircle may originate from the presence of distribution in relaxation time within the bulk response. The radius of the semicircle decreases with increasing temperature due to the increase in the conductivity of the sample. At higher temperature the electrode effect becomes predominant, with a spike at lower frequencies. Our experimental results suggest that the depressed semicircles in the impedance spectra correspond to the bulk behavior of the sample, as will be explained below, and there is no grain boundary contribution to the impedance spectra. Two equivalent circuits appropriate to these plots are shown in the inset of figure 5 according to the temperatures range. Below 330K we have performed a simulation of an equivalent circuit consisting only of two Rp1// CPE1 and Rp2// CPE2 elements connected in series as shown in the inset of figure6 which corresponding to the bulk and electrode effects, respectively. Above 330K a constant phase element CPE3 acting as a blocking double layer capacitance is added in series to the former equivalent circuit

The real and imaginary components of the whole impedance of this circuit were calculated according to the following expressions:

- T<330K

$$Z' = \frac{R_{p1}^2 Q_1 \omega^{\alpha 1} \cos\left(\frac{\alpha_1 \pi}{2}\right) + R_{p1}}{\left(1 + R_{p1} Q_1 \omega^{\alpha 1} \cos\left(\alpha_1 \frac{\pi}{2}\right)\right)^2 + \left(R_{p1} Q_1 \omega^{\alpha 1} \sin(\alpha_1 \frac{\pi}{2}\right)^2} + \frac{R_{p2}^2 Q_2 \omega^{\alpha 2} \cos\left(\frac{\alpha_2 \pi}{2}\right) + R_{p2}}{\left(1 + R_{p2} Q_2 \omega^{\alpha 2} \cos\left(\alpha_2 \frac{\pi}{2}\right)\right)^2 + \left(R_{p2} Q_2 \omega^{\alpha 2} \sin(\alpha_2 \frac{\pi}{2})\right)^2} \quad (4)$$

$$Z''=\frac{R_{p1}^2 Q_1 \omega^{\alpha 1}\sin(\frac{\alpha_1\pi}{2})}{\left(1+R_{p1}Q_1\omega^{\alpha 1}\cos\left(\alpha_1\frac{\pi}{2}\right)\right)^2+\left(R_{p1}Q_1\omega^{\alpha 1}\sin\left(\alpha_1\frac{\pi}{2}\right)\right)^2}+\frac{R_{p2}^2 Q_2 \omega^{\alpha 2}\sin(\frac{\alpha_2\pi}{2})}{\left(1+R_{p2}Q_2\omega^{\alpha 2}\cos\left(\alpha_2\frac{\pi}{2}\right)\right)^2+\left(R_{p2}Q_2\omega^{\alpha 2}\sin\left(\alpha_2\frac{\pi}{2}\right)\right)^2} \quad (5)$$

where Rp is the bulk resistance and the impedance of CPE is $z_{CPE}=1/Q(i\omega)^{\alpha}$, where Q indicates the value of capacitance of the CPE element and α is the fractal exponent.

- T>330K

$$Z''=\frac{R_{p1}Q_1\omega^{\alpha 1}\cos(\frac{\alpha_1\pi}{2})+R_{p1}}{\left(1+R_{p1}Q_1\omega^{\alpha 1}\cos(\alpha_1\frac{\pi}{2})\right)^2+\left(R_{p1}Q_1\omega^{\alpha 1}\sin(\alpha_1\frac{\pi}{2})\right)^2}+\frac{R_{p2}Q_2\omega^{\alpha 2}\cos(\frac{\alpha_2\pi}{2})+R_{p2}}{\left(1+R_{p2}Q_2\omega^{\alpha 2}\cos(\alpha_2\frac{\pi}{2})\right)^2+\left(R_{p2}Q_2\omega^{\alpha 2}\sin(\alpha_2\frac{\pi}{2})\right)^2}+\cos\left(\frac{\alpha_3\pi}{Q_3\omega^{\alpha 3}}\right) \quad (6)$$

$$Z''=\frac{R_{p1}^2 Q_1\omega^{\alpha 1}\sin(\frac{\alpha_1\pi}{2})}{(1+R_{p1}Q\omega^{\alpha 1}\cos(\alpha_1\frac{\pi}{2}))^2+\left(R_{p1}Q_1\omega^{\alpha 1}\sin\left(\alpha_1\frac{\pi}{2}\right)\right)}+\frac{R_{p2}^2 Q_2\omega^{\alpha 2}\sin\left(\frac{\alpha_2\pi}{2}\right)}{(1+R_{p1}Q\omega^{\alpha 1}\cos(\alpha_1\frac{\pi}{2}))^2+\left(R_{p1}Q_1\omega^{\alpha 1}\sin\left(\alpha_1\frac{\pi}{2}\right)\right)}+\frac{\sin\left(\frac{\alpha_3\pi}{2}\right)}{Q_3\omega^{\alpha 3}} \quad (7)$$

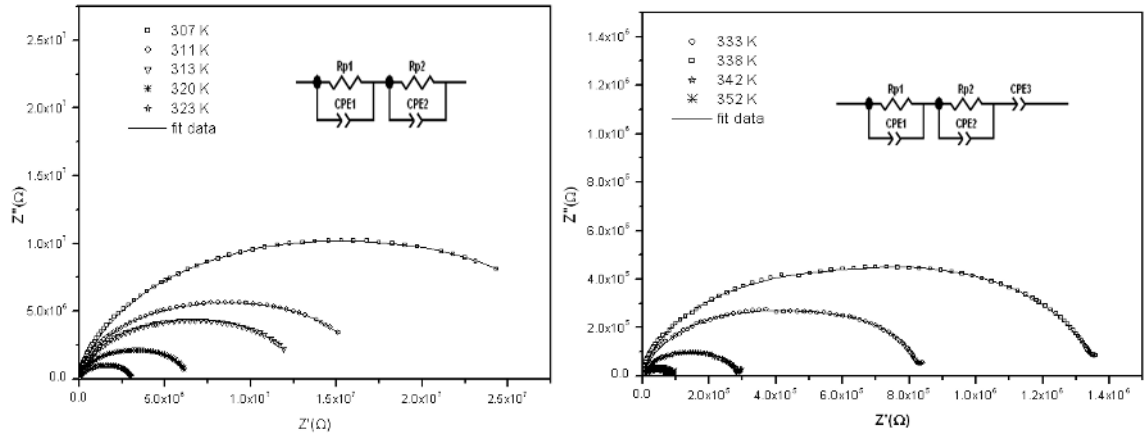

Fig.6. Experimental and simulation impedance data for $[C_2H_{10}N_2]Cd(SCN)_2(Cl)_2$ at different temperatures. The insets show the proposed equivalent circuits.

Moreover figure 7 shows a good agreement between the experimental and simulation results of the real and the imaginary parts of impedance us function of frequency.

Additionally, the capacitance values calculated at the maximum frequency, ω_{max}, at Z'' peaks using the relation ω_{max} RC=1 are reported in Table 3.

These low capacitances values (pF order) are usually assigned to grain response rather than grain boundary, whose higher capacitance value is the nF-**μ**F order [10]

Table 3. Temperature dependence of Rp, Q, and the fractional exponent α.

T<330K								
T(K)	$R_{p1}(10^6\Omega)$	α_1	Q_1(pF)	$R_{p2}(10^6\Omega)$	α_2	Q_2(pF)		
307	18.59	0.830	26.9	11.89	0.91	96.2		
311	10.70	0.836	90.7	6.49	0.88	21.8		
313	7.70	0.840	96.3	5.47	0.87	24.2		
315	5.67	0.850	103	4.43	0.86	26.0		
320	2.76	0.860	31	3.71	0.83	11.6		
T>330K								
T(K)	$R_{p1}(10^5\Omega)$	α_1	Q_1(pF)	$R_{p2}(10^5\Omega)$	α_2	Q_2(pF)	α_3	$Q_3(10^{-7}F)$
333	3.410	0.930	98	4.880	0.860	31.1	0.670	1.60
336	2.370	0.890	135	3.120	0.870	31.9	0.750	1.14
342	1.68	0.850	150	1.19	0.910	23.9	0.710	1.87
352	0.38	0.810	53	0.45	0.930	19.2	0.810	1.16

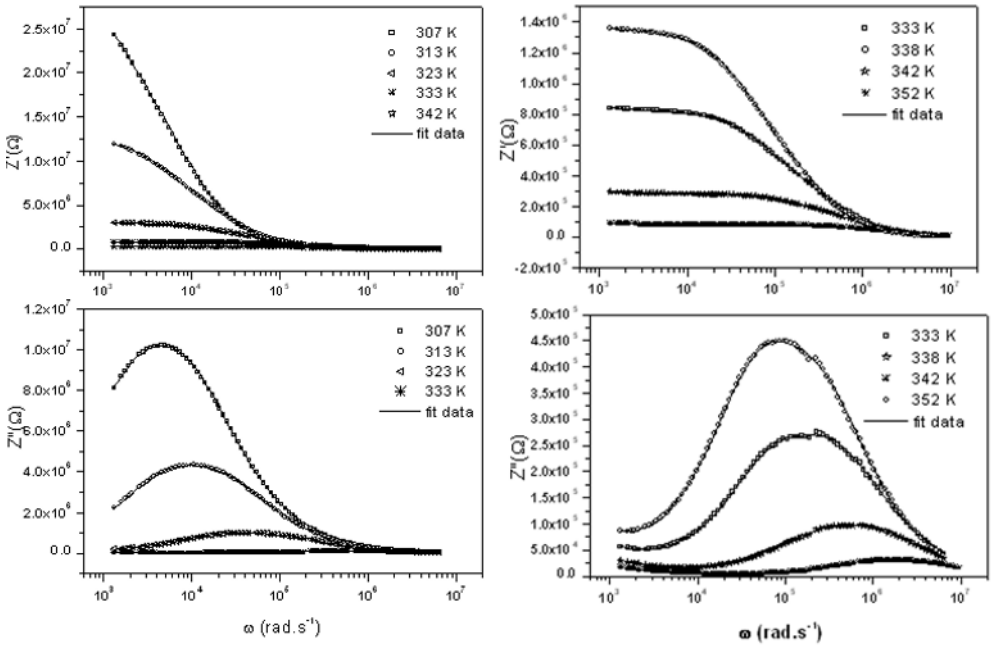

Fig.7. Frequency dependence of the Z' and Z'' of $C_2H_{10}N_2Cd(SCN)_2(Cl)_2$ at various temperatures

3.4 Conductivity

The electrical conductivity at each temperature was obtained by using the formula σ_p= L/Rp.A where Rp is the bulk resistance of the sample, at each temperature was obtained from the intercept of the semicircular portion on the real axis, L is the thickness and A is the area of cross section of the sample. Figure8 shows the electrical conductivity vs-reciprocal temperature of polycrystalline $C_2H_{10}N_2Cd(SCN)_2(Cl)_2$ between 300 and 370 K during heating run. The activation energy obtained from the slope of the straight line segment using the Arrhenius known relationship:

$$\sigma_p.T=\sigma_0 \exp\frac{-\Delta E_a}{k_B.T} \tag{8}$$

where σ_p is the electrical conductivity at temperature T, σ_o the pre-exponential factor, k_B the Boltzmann's constant and ΔE_a is the thermal activation energy for the ion migration yield to ΔE_a=(0.540 (3)) eV and σ_o=3.3510×10$^6\Omega^{-1}$cm^{-1}K.

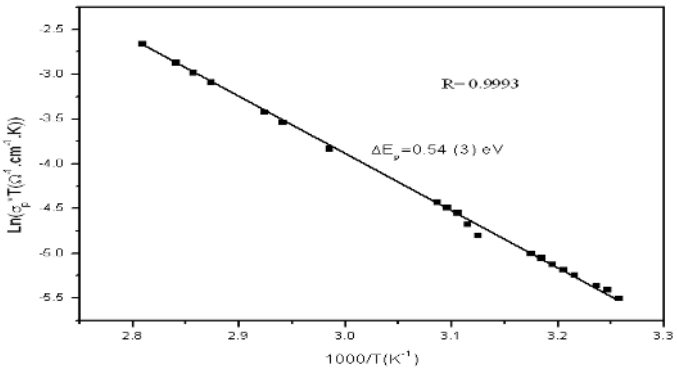

Fig.8. Variation of Ln(σ_p.T) versus (1000/T) of $C_2H_{10}N_2Cd(SCN)_2(Cl)_2$

3.5 Dielectric studies

The complex permittivity can be expressed as a complex number $\varepsilon^*(\omega) = \varepsilon'(\omega) - i\,\varepsilon''(\omega)$. The dielectric relaxation is described by a non-Debye model which gives the frequency dependent complex permittivity in the form [11]:

$$\varepsilon^*(\omega) = \varepsilon' + i\varepsilon'' = \varepsilon_\infty + \frac{\varepsilon_S - \varepsilon_\infty}{1+\left(\frac{i\omega}{\omega_1}\right)^{1-\alpha}} + \frac{\sigma_0}{i\varepsilon_0\omega} \tag{9}$$

where σ_o represents the specific conductivity of the title compound, ε_s is the static permittivity, ε_0 is the permittivity of the free space, ε_∞ is the high frequency value of ε'' and ω_1 is the relaxation angular frequency of the Debye process. The real part of $\varepsilon'(\omega)$ and the imaginary part of $\varepsilon''(\omega)$ are expressed by:

$$\varepsilon'(\omega) = \varepsilon_\infty + \frac{(\varepsilon_s - \varepsilon_\infty)\left[1+(\frac{\omega}{\omega_1})^{1-\alpha}\cos\left(\frac{(1-\alpha)\pi}{2}\right)\right]}{1+2\left(\frac{\omega}{\omega_1}\right)^{1-\alpha}\cos\left(\frac{(1-\alpha)\pi}{2}\right)+\left(\frac{\omega}{\omega_1}\right)^{2(1-\alpha)}} \tag{10}$$

$$\varepsilon''(\omega) = \frac{(\varepsilon_S - \varepsilon_\infty)\left(\frac{\omega}{\omega_1}\right)^{1-\alpha}\sin(1-\alpha)\frac{\pi}{2}}{1+2\left(\frac{\omega}{\omega_1}\right)^{1-\alpha}\cos\left((1-\alpha)\frac{\pi}{2}\right)+\left(\frac{\omega}{\omega_1}\right)^{2(1-\alpha)}} + \frac{\sigma_0}{\varepsilon_0\omega} \tag{11}$$

The first part in Eq.11 refers to the thermal polarization and the second one to the electrical conductivity [12]. Consequently, the loss factor is calculated as follows:

$$\tan(\varepsilon(\omega)) = \varepsilon''(\omega) / \varepsilon'(\omega) \quad (12)$$

The frequency dependence of the dielectric function of a solid reflects the dynamic response of the constituents of the solid. Figure 9 shows that the dielectric constant decreases with increase in frequency. At low frequency due to space charge accumulation a gradual increase in the dielectric constant have been observed. At higher frequencies the change in the direction of the electric field lines is too fast to be followed by the charged ion and hence the dielectric constant decreases.

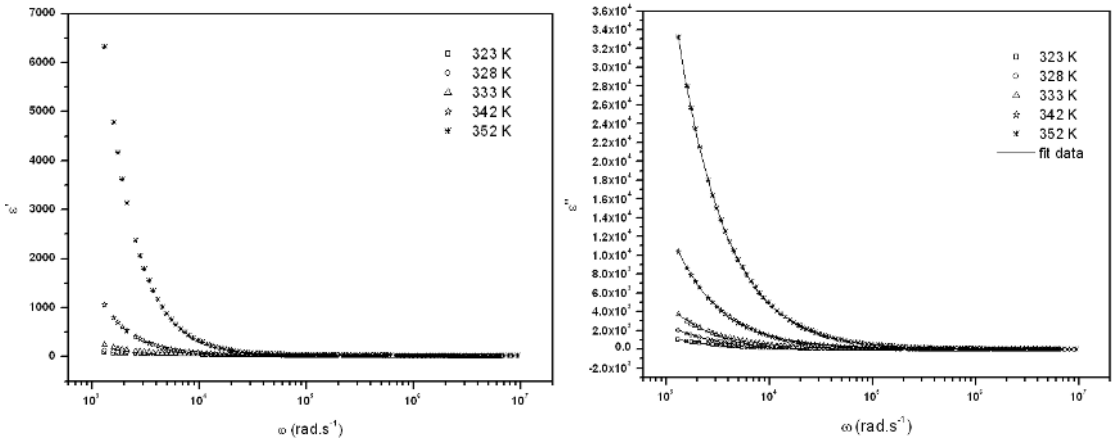

Fig.9. Frequency dependence of the real part (ε') and the imaginary part permittivity (ε") with the best fitted data of complex permittivity of $C_2H_{10}N_2Cd(SCN)_2(Cl)_2$ at various temperatures

Figure 9 shows also the frequency dependence of the imaginary part of the dielectric constant from fitting Eq. (11). There are no appreciable relaxation peaks in the frequency range employed in this study. The dielectric loss rises sharply at low frequency indicating that electrode polarization and space charge effects have occurred confirming non-Debye dependence [13]. The dielectric loss increases at higher temperatures due to the higher charge carrier density. The least squares fit parameters obtained for different temperatures are shown in Table 4.

Table 4. Least squares fit parameters of the imaginary part of permittivity (ε")

T(K)	ω_1(rad.s^{-1})	α	σ_o(Ω^{-1}cm^{-1})
323	1053	0.68	$1.23.10^{-7}$
328	1595	0.50	$2.12.10^{-7}$
333	2550	0.67	$3.51.10^{-7}$
342	7214	0.70	$1.05.10^{-6}$
352	25180	0.50	$3.6.10^{-6}$

Figure10 exhibits loss tangent tan(ε) variation with angular frequency and temperatures. The maximum in the tan(ε) peak shifts to higher frequency with rise of temperature. We noticed clearly that larger tan (ε) values are for higher temperatures. The tan (ε) increases with rise in frequency and showed a maximum at particular angular frequency ωp for different temperatures because the active component (ohmic) of the current increases more rapidly than its reactive component (capacitive). At higher frequencies tan(ε) decreases with increasing frequency because the active component of the current is practically independent of frequency and the reactive component increases in proportion to the frequency [14].

With respect to the different temperatures, the relaxation time, τ_t, is calculated according to the resonance condition, which is defined by $\omega_t\tau_t=1$ from the peak maximum of tan(ε). The temperature dependence of τ_t is plotted in figure 11. It is well described by the Arrhenius relation:

$$\tau_t = \tau_0 \exp\left[-\frac{\Delta E_t}{k_B.T}\right] \tag{13}$$

where τ_0 is the characteristic relaxation time and ΔE_t is the activation energy for the relaxation process, k_B is the Boltzmann constant and T is the absolute temperature. The activation energy ΔE_t obtained from the loss tangent is about of (ΔE_t =0.530(3)) eV.

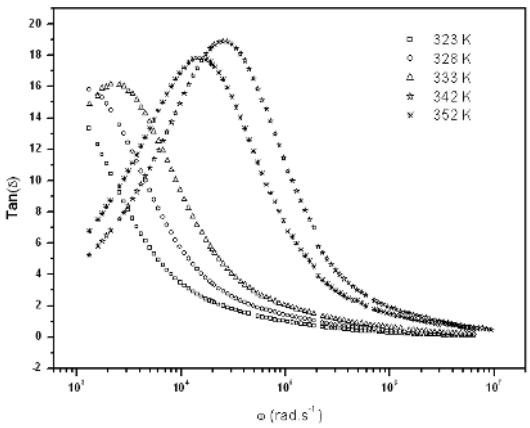

Fig.10. Frequency dependence of tan(δ) at various temperatures

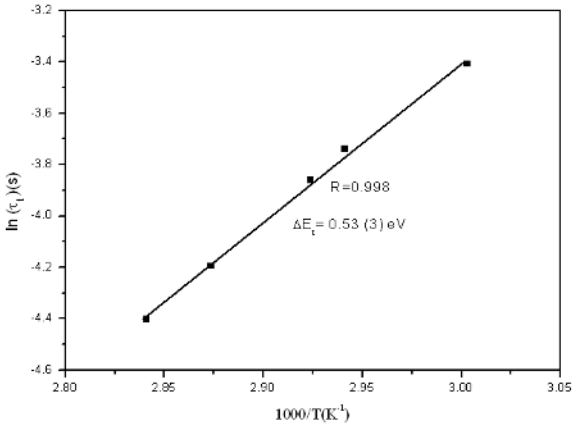

Fig.11. Variation of the relaxation time (τ_t) versus (1000/T)

The activation energy for conduction (ΔE_a=(0.540(3)eV) is almost the same as that of the activation energy for the relaxation process (ΔE_t =0.530(3)) eV. The near value of activation energies obtained from the analyses of conductivity data and circuit equivalent confirms that the conductivity deduced from the impedance arcs is dominated by the grain-interior conductivity, characterized by the hopping mechanism [15].

Conclusions

The crystalline complex was prepared and studied by mean single crystal X-ray diffraction, heteronuclear ^{111}Cd, ^{13}C CP/MAS NMR spectroscopy and impedance spectroscopy. The structure shows a layer arrangement: planes of $[CdCl_2(SCN)_2]_n^{2-}$ chains alternate with planes of $[(NH_3)_2(CH_2)_2]^{2+}$. The cadmium atoms are bridged by two thiocyanate ions generating 1-D polymeric-chains. These chains are themselves interconnected by means of N-H…Cl (NCS) hydrogen bonds originating from the organic cation $[(NH_3)_2(CH_2)_2]^{2+}$. The isotropic region of the ^{111}Cd CP/MAS NMR spectrum of $[C_2H_{10}N_2]CdCl_2(SCN)_2$ shows spin-spin coupling of ^{111}Cd with two ^{14}N indicates the presence of two equivalent thiocyanate ligands, in agreement with the results of the single crystal X-ray diffraction. Examination of the ^{13}C CP/MAS NMR line shapes allows direct measurement of the ^{13}C, ^{14}N dipolar coupling constant of 1381Hz. The analysis as function of temperatures of the frequency dispersion of the real and the imaginary components of the complex impedance allowed determining two equivalent circuits for this material. The near value of activation energies obtained from the analysis of the conductivity data and the equivalent circuit confirms that the transport is through ion hopping mechanism in the investigated material.

Acknowledgments

The authors would like to thank Dr. K. Eichele holder of the Department of Chemistry of Canada, for many helpful discussions and his assistance for the calculus of the simulated spectra.

References

1. R. W. Asmussen and O. Bostrup, Acta Chem.Scand, **11** (1957)
2. G. M. Sheldrick, SHELXL PLUS.PC Version; a system of computer programs for the determination of crystal structures from X-ray diffraction data, Rev.**5** (1998)
3. L. J. Farrugia, WinGX program for crystallography package. J. App. Cryst **32** (1999)
4. Mercury 2.3; a Crystal Structure Visualization and Exploration belonging to the Cambridge Crystallography Data Centre (CCDC)
5. International Tables for X-Ray Crystallography, Vol. **II**, *Kynoch Press, Birmingham* (1959)
6. K. Eichele, R. E. Wasylishen, J. Inorg. Chem. **33** (1994)
7. S. Andrew Lipton, S. Scott. Mason, Daniel L. Reger, and D. Paul Ellis, J. Am. Chem. Chem. Soc**. 116** (1994)
8. A. C. Olivieri, L. Frydman, L. E. Diaz, J. Magn. Reson (1987)
9. G. M. Tsangaris, G. C. Psarras and N Kouloumbi, J. Mater. Sci.**33** (1998)
10. Ye. Haittao, C. Sun, Hung d, P. Hing, *Thin Solid Films* **381** (2001)
11. B. Louati, K. Guidara, M. Gargouri Phys. Status. Solidi. **B241** (2004)
12. N. Ponpandian, P. Balaya, and A. Narayanasamy, J. Phys. Condens. Mater **14** (2002)
13. X. Qian, N. Gu, Z. Cheng, X. Yang, S. Dong, Electrochim. Acta **46** (2001)
14. F. Erragh, A. Boukhari, B. Elouadi and F. Abraham, J. Solid State Chem. **120** (1995)
15. A. Ben Rhaiem. N. Zouari. K. Guidara. M. Gargouri. A. Daoud, J. Alloys Compd. **387** (2005)